Planetary and Space Science 59 (2011) 1498–1505

Contents lists available at ScienceDirect

Planetary and Space Science

journal homepage: www.elsevier.com/locate/pss

A statistical study of flux ropes in the Martian magnetosphere

J.A. Briggs [a,*], D.A. Brain [a], M.L. Cartwright [a], J.P. Eastwood [b], J.S. Halekas [a]

[a] Space Sciences Laboratory, University of California Berkeley, Berkeley, CA 94720, USA
[b] Blackett Laboratory, Imperial College London, London SW7 2AZ, UK

ARTICLE INFO

Article history:
Received 7 January 2011
Received in revised form
9 May 2011
Accepted 14 June 2011
Available online 29 June 2011

Keywords:
Mars
Plasma interaction
Magnetic fields
Flux ropes

ABSTRACT

Using minimum variance analysis of the circular mapping data from the Mars Global Surveyor (MGS) spacecraft during four selected weeks of observation, we identify 360 magnetic field structures in the Martian topside ionosphere with characteristic signatures of flux ropes. Physical parameters including size, peak field strength, helicity, orientation, and external conditions at the time of each observation are compiled for the events in each population. We observe that Martian flux ropes typically have a peak field amplitude of ~15 nT and a diameter of ~80–100 km assuming they are stationary. Flux ropes tend to be aligned approximately parallel to the planetary surface, and perpendicular to the direction from which the solar wind flows. They are more frequently observed during times of low solar wind pressure, but do not show a clear preference for a particular Interplanetary Magnetic Field (IMF) draping direction. Flux rope characteristics of peak field amplitude, diameter, and helicity vary with solar zenith angle. Amplitudes tend to be higher during periods of high solar wind pressure. The events are sorted into three populations based on the location at which they were observed, possibly corresponding to distinct formation mechanisms. Flux ropes observed in eclipse tend to have smaller peak amplitudes and are larger than those observed in sunlight, and are less likely to be oriented parallel to the planetary surface. Proximity to crustal fields does not appear to influence the characteristics of flux ropes observed at the 400 km spacecraft altitude. The frequent observation of flux rope structures near Mars in a variety of locations suggests that the low-altitude plasma environment is quite dynamic, with magnetic shear playing a prominent role in determining magnetic field structure near the planet.

1. Introduction

Magnetic flux ropes are regions of twisted magnetic field, thought to form as a consequence of magnetic shear or reconnection. Russell and Elphic (1979) described magnetic flux ropes as being twisted around a central axis; magnetic field far from the axis is weak and azimuthal and magnetic field close to the axis is stronger and axially oriented. Flux ropes interact with planetary and interplanetary charged particles, and can transport large volumes of plasma. Flux ropes are therefore of interest to those who wish to understand energy and particle transport in space plasmas.

Flux ropes (sometimes called by different names, including plasmoids, magnetic clouds, and flux transfer events) have been observed in a variety of locations throughout the solar system, including Earth's magnetosphere (e.g. Russell and Elphic, 1978; Hones et al., 1984; Sibeck et al., 1984; Elphic et al., 1986), the solar wind (e.g. Bulraga et al., 1981; Moldwin et al., 1995), Mercury (Slavin et al., 2009), Venus (e.g. Russell and Elphic, 1979), Mars (e.g. Cloutier et al., 1999), Jupiter (e.g. Walker and Russell, 1985; Kronberg et al., 2005), Saturn (e.g. Jackman et al., 2007, 2008), and Titan (Wei et al., 2010). The processes that result in their formation are clearly ubiquitous.

Three varieties of flux rope have been reported in the Martian topside ionosphere and magnetosphere, at altitudes ranging from more than 1000 km down to the typical altitude of the ionospheric main peak, near 120 km. Ionospheric flux ropes similar to those discovered at Venus were measured by Mars Global Surveyor (Cloutier et al., 1999; Vignes et al., 2004). Ionospheric flux ropes are relatively small (10's km across), with peak magnetic field amplitude comparable to the strength of the magnetic field draped around the ionosphere (10's nT). They are thought to form shear-related instabilities between shocked solar wind plasma and the ionosphere, at times when the ionospheric thermal pressure exceeds the solar wind dynamic pressure (i.e. when the ionosphere is unmagnetized) (cf. Luhmann, 1990). According to Vignes et al. (2004), ionospheric flux ropes at Mars are observed less frequently and with more random orientations than at Venus, and appear mostly in the northern hemisphere (in regions of low crustal magnetization).

* Corresponding author.
E-mail address: jabriggs87@gmail.com (J.A. Briggs).

0032-0633/$ - see front matter © 2011 Elsevier Ltd. All rights reserved.
doi:10.1016/j.pss.2011.06.010

A second variety of flux rope, likely analogous to plasmoids in Earth's magnetotail, has been identified downstream from the strong Martian crustal fields in the Southern hemisphere (Brain et al., 2010; Morgan et al., 2011). These flux ropes are much larger (100's km across) and stronger (as high as 200 nT) than ionospheric flux ropes, and are proposed to form as crustal field lines are stretched tailward by the shocked solar wind. Morgan et al. (2011) showed that these features are quasi-steady for time periods of 30 min or more, and Brain et al. (2010) propose that the stretched crustal field lines detach, carrying ionospheric plasma with them in a bulk atmospheric escape process. These observations support the results of global plasma simulations (Harnett, 2009), which showed the formation of large, strong flux ropes associated with crustal fields. The simulated flux ropes have short lifetimes, analogous to flux ropes in Earth's magnetotail, and carry planetary ions accelerated by the electric field in the rope.

Finally, Eastwood et al. (2008) have identified flux ropes near current sheets on the nightside of Mars. They are small and weak, like the ionospheric flux ropes observed on the dayside. However, based on their association with Hall magnetic field signatures near current sheets, these flux ropes likely result from collisionless magnetic reconnection, analogous to magnetotail flux ropes observed in Earth's plasma sheet (e.g. Elphic et al., 1986; Slavin et al., 2003; Eastwood et al., 2005, 2007). Magnetic reconnection is an active process at Mars, even far from crustal magnetic fields (Eastwood et al., 2008; Halekas et al., 2009).

The only previous statistical study of flux ropes at Mars, by Vignes et al. (2004) considered that all flux ropes occurring there were Venus-like ionospheric flux ropes, and used data from the MGS elliptical pre-mapping orbits. These orbits provided good coverage of large portions of the Martian plasma interaction region at a variety of altitudes and local times—though coverage at low altitudes for the period considered by Vignes et al. (2004) was best in the northern hemisphere. Here we undertake a new statistical study of flux ropes at Mars, cognizant that several types of flux rope occur near the planet. We use observations from the MGS mapping orbits, which provided good coverage of both hemispheres in a narrow local time and altitude range (near 400 km). In the next section we discuss the MGS observations and present a single flux rope event. Next, we present the results of a statistical analysis of MGS data. Finally, we present a simple upper-limit estimate of the atmospheric loss that may result via flux ropes at Mars.

2. Identification of flux ropes in MGS data

We use observations from the MGS magnetometer (MAG) made while the spacecraft was in a nearly circular mapping orbit with altitude of ~400 km, fixed in local time at 2 am/2 pm. MAG provided vector magnetic field data every 0.75, 1.5, or 3.0 s (depending upon the spacecraft telemetry rate) with an accuracy of 0.5–1.0 nT, (Acuña et al., 2001). This data rate and accuracy are sufficient for detecting even relatively small (10–20 km) and weak (10 nT) magnetic field features.

A time-series of MAG data from a representative 15-min time period is plotted in Fig. 1a. During this time MGS was above the dayside northern hemisphere (Fig. 1b), and measured peaks in the electron energy spectrum (not shown) characteristic of ionospheric photoelectrons (Mitchell et al., 2000) indicating that the spacecraft was in the high altitude ionosphere. The measured field magnitudes during this period were much lower than the typical ~30 nT draped solar wind field typical for this region (Brain et al., 2003). There are a number of short-duration (~30–60 s) enhancements in the field magnitude, each accompanied by a field rotation. These enhancements are too short in duration to be nearby weak crustal fields.

In order to determine whether these features have magnetic field geometry consistent with flux ropes, minimum variance analysis (MVA) (Sonnerup and Cahill, 1967) is applied. Fig. 2a shows the magnetic field components in MVA coordinates for the event at 06:58 highlighted in red in Fig. 1a. Most of the variation in the magnetic field occurs in a plane defined by the maximum and intermediate eigenvectors (the eigenvalues are 44, 26, and 1.0). Hodograms (Fig. 2b) show that the field undergoes a circular rotation in this plane, with small but repeatable variation in the minimum variance direction. These features are very similar to those shown previously for flux ropes in a number of settings, including those first identified in the Venus ionosphere (Russell and Elphic, 1979). We therefore identify this feature as a flux rope. It should be noted that the axis of the flux rope corresponds to the eigenvector whose magnetic field does not change sign. In an ideal case (where the spacecraft passes close to the center of a force-free flux rope), this is the intermediate variance direction (Lepping et al., 1990). In practice, if the eigenvalues of the maximum and intermediate variance directions are similar, MVA may result in the axis aligning along the maximum variance direction, as is the case here. A number of other magnetic field enhancements coincident with field rotations are identified as flux ropes and highlighted in orange in Fig. 1a.

Using the example from Fig. 2a we can identify a number of characteristics of the flux rope. The peak amplitude sampled by the spacecraft was ~20 nT in the flux rope. However, it is likely that the spacecraft did not pass through the center of the structure, and so the true peak field amplitude in the flux rope should be at least a little larger than 20 nT. If we assume the central axis of the flux rope is in the same direction as the maximum eigenvector (associated with field measurements that do not change sign), then the rope is inclined ~30° to the local horizontal, and ~80° to the sunward direction. Considering the transit time of the spacecraft through the magnetic field structure, we derive a diameter of ~110 km, assuming that the flux rope was stationary and the spacecraft passed through the center of the flux rope. If we instead assume that the flux rope is moving anti-planetward relative to the spacecraft at modest (few km/s) speeds then we obtain a larger diameter of ~180 km. Since we do not know the absolute motion of the flux rope, we simply calculate the 'stationary size', in this case 110 km, as a first attempt to determine a fiducial estimate of flux rope size. Finally, we compute the flux rope's helicity (a measure of how tightly coiled the rope is) to be 1.75, given by the ratio of the maximum to intermediate eigenvalue obtained from MVA (Vignes et al., 2004). Helicity close to unity implies a 'stretched' rope, while larger helicity indicates a more tightly coiled rope.

We have examined four one-week periods, evenly spaced over a year (the first week in each of July 1999, October 1999, January 2000, and April 2000) for the presence of flux rope features similar to those discussed above. Since MGS orbited Mars every ~2 h, a total of ~84 orbits were examined in each of the four intervals. From this subset of the observations we identified thousands of roughly symmetric increases in magnetic field magnitude accompanied by field rotations, avoiding obvious large-scale crustal fields. MVA was applied to each candidate event to determine if the field variation was consistent with the expected geometry of a flux rope, similar to that illustrated in Fig. 2.

Events included in this initial survey of the MGS mapping dataset satisfied the following criteria in addition to the roughly symmetric increase in magnetic field magnitude. First, guided by the results of Ledvina et al. (2002) that force-free flux ropes have circular (and not elliptical) hodograms in the maximum-intermediate plane, we accepted only events with nearly circular hodograms in the MVA i–j component. Next, we required that

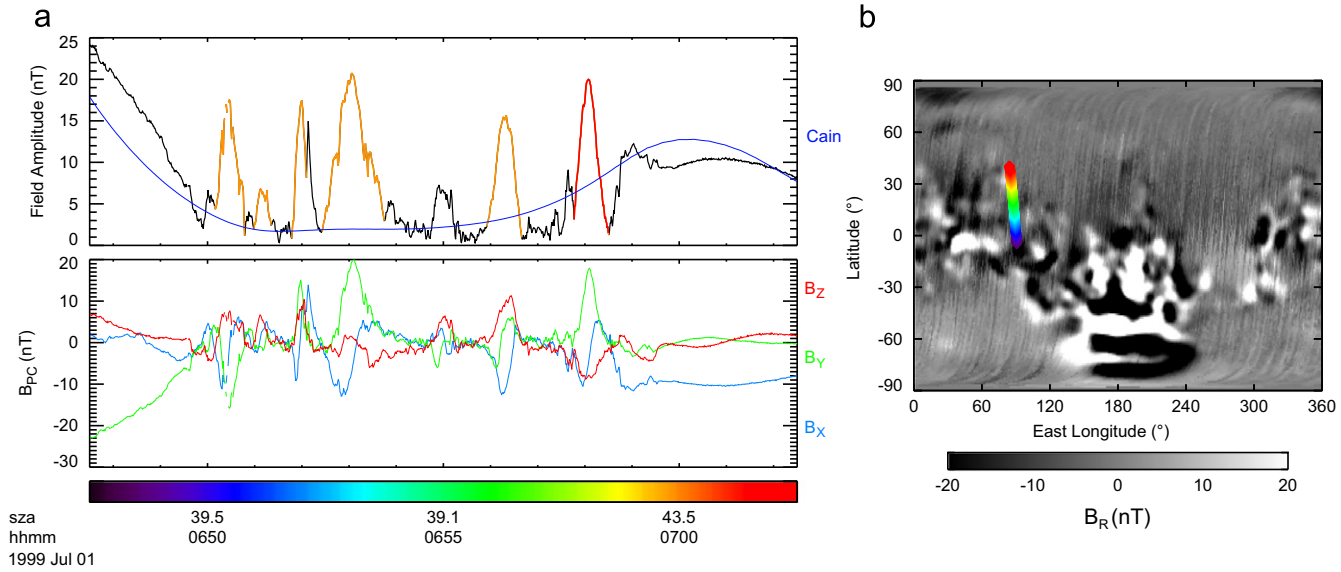

Fig. 1. (a) Time-series magnetic field data (magnitude [top] and planetary cartesian coordinates [bottom]). Field magnitude from a crustal field model by Cain et al. (2003) is shown in blue. Features identified as flux ropes are shown in orange. The flux rope presented in Fig. 2 is shown in red. (b) MGS orbit trajectory (colored by time) at ~400 km altitude plotted over the median radial field component measured by MGS on the nightside (shaded in greyscale). (For interpretation of the references to color in this figure legend, the reader is referred to the web version of this article.)

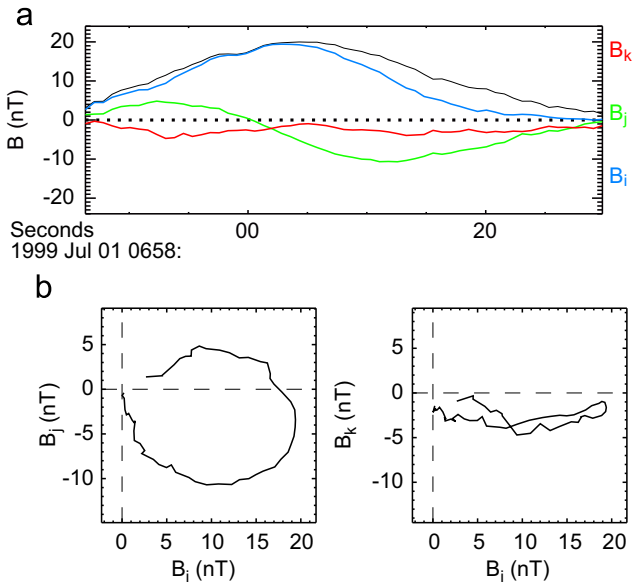

Fig. 2. (a) Magnetic field components in minimum variance coordinates (magnitude shown in black) for the feature highlighted in orange in Fig. 1a. B_i (blue), B_j (green), and B_k correspond to the maximum, intermediate, and minimum variance components. (b) Hodograms for the same time period, in MVA coordinates. (For interpretation of the references to color in this figure legend, the reader is referred to the web version of this article.)

either the maximum or intermediate MVA field component have a bipolar signature, indicating a change in direction of one of the field components (the remaining maximum or intermediate component must be mono-directional). There are many magnetic field structures evident in MGS data that have a circular hodogram but lack a bipolar field component. Such structures may, for example, result from waves or traveling compression regions. Finally, we required that the ratio of intermediate to minimum eigenvalue be at least eight, ensuring that most of the field variation occurs in a single plane. A similar criterion, derived by testing MVA against multi-spacecraft analysis has been used elsewhere (e.g. Knetter et al., 2004; Eastwood et al., 2002). For reference, the event shown in Fig. 2 has eigenvalue ratio of 28, well above the cutoff value. These constraints may exclude many flux ropes near Mars that are not fully formed or that are not in force balance (the second constraint excluded 31 additional examples that we had identified as possible events), but our effort here is focused on including only relatively certain examples of flux ropes for a first analysis.

We identified 360 flux rope events that satisfied our selection criteria in this four-week period (219, 32, 56, and 53 in each of the four weeks), significantly increasing the database of flux rope events for Mars. The location and peak amplitude for each flux rope are plotted in Fig. 3. Few or no flux ropes were identified over strong crustal fields. Contrary to the results of Vignes et al. (2004), we are able to identify flux ropes in the southern hemisphere. However, more ropes were identified in the northern hemisphere than in the southern hemisphere, even when comparing only regions lacking significant crustal magnetization. The peak field amplitude measured in each flux rope ranges from ~3–100 nT.

As discussed in Section 1, three different types of flux rope have been reported for Mars, and each may have different formation mechanisms. It is relatively difficult at present to distinguish one type of flux rope from another for any single example. However, noting that the three previously reported types of flux rope are often expected to occur in different locations, we have made a preliminary attempt to divide our sample into three populations based on the location of each rope. Population 1 (217 events) consists of ropes observed in sunlight and far from crustal fields, expected for Venus-like ionospheric flux ropes. Population 2 (80 events) consists of ropes observed in sunlight within 10° (angular separation as measured from the center of Mars) of crustal fields. Population 3 (63 events) consists of ropes observed in eclipse. By testing whether the characteristics of one population differ significantly from another we hope to infer whether the formation and/or evolution processes of each population are distinct from each other.

From Fig. 3, we see that many of the weakest flux ropes are observed in eclipse in the northern hemisphere. Several of the strongest flux ropes are associated with crustal fields (defined

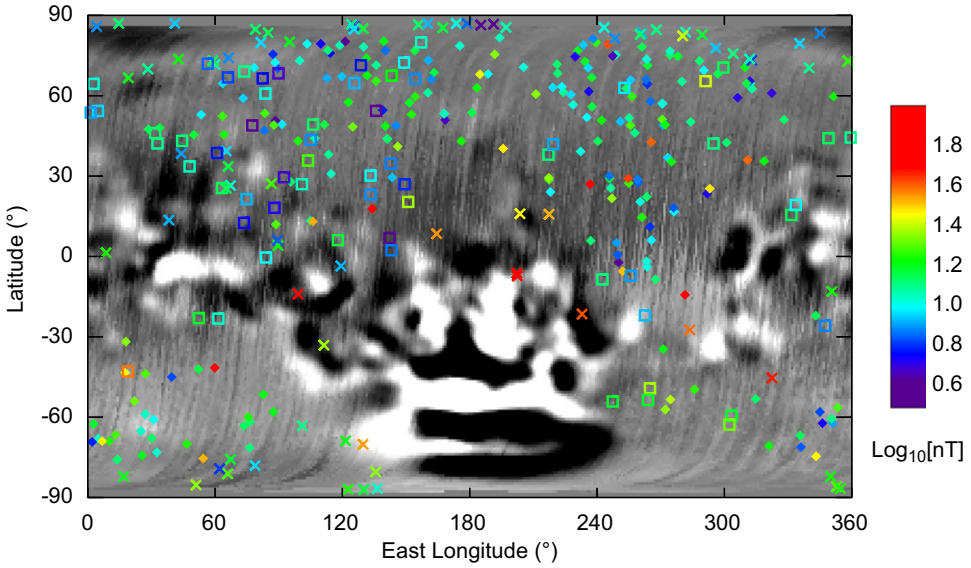

Fig. 3. Location of each flux rope, colored according to the logarithm of the peak field amplitude measured in the rope. Symbols denote the population assigned to each rope: diamonds for population 1, crosses for population 2, and squares for population 3. The map is shaded in grayscale similar to Fig. 1b. (For interpretation of the references to color in this figure legend, the reader is referred to the web version of this article.)

Table 1
Statistics for flux rope parameters. Median, mean, and standard deviations of each parameter are provided for all flux ropes (left) and for each of the three populations defined in the text (right).

Parameter	Median		Mean		Std. dev.	
Peak amplitude (nT)	13.0	13.5	15.1	15.5	11.1	11.5
		13.7		16.9		12.2
		10.5		11.6		6.5
Stationary size (km)	80.5	70.7	106.7	101.0	97.2	103.3
		81.3		101.0		65.3
		104.1		133.2		105.9
Incl. w.r.t local horizontal (deg.)	23.9	21.7	28.7	27.1	20.4	19.8
		23.4		27.1		20.1
		37.0		36.2		21.5
Incl. w.r.t. sunward direction (deg.)	55.9	56.0	54.9	56.4	21.8	21.0
		55.7		53.4		22.7
		53.5		51.5		23.4
Helicity	1.88	1.89	2.30	2.35	1.45	1.47
		1.90		2.24		1.31
		1.78		2.21		1.58

here as having field magnitude of 20 nT or more at the MGS 400 km mapping altitude), but many weaker flux ropes are also observed near crustal fields.

3. Statistical analysis

Using the 360 flux ropes identified in Section 2, we proceed with a statistical analysis of their intrinsic characteristics and the external conditions at the time they were identified. For each event we extract the peak field strength, the direction of the central axis of the flux rope (associated with whichever of the maximum and intermediate field components does not change sign), and the flux rope 'stationary size' and helicity as described in Section 2. Table 1 shows mean and median values for several flux rope parameters for the entire population of events, and separately for each of the three populations defined in Section 2: dayside flux ropes far from crustal fields (population 1), dayside flux ropes close to crustal fields (population 2), and nightside flux ropes (population 3).

From the table we see that a 'typical' flux rope at Mars has peak amplitude of ~15 nT, and is ~80 km in size. It lies at low angles to the local horizontal and intermediate angles to the Mars–Sun direction. However, Table 1 also indicates that there is a large range in values for several of the parameters. The typical values of each parameter are similar among the different populations, within the uncertainty. However, flux ropes observed in eclipse (population 3) may have lower amplitude, larger size, and be more inclined to the local horizontal than ropes from other populations.

Fig. 4 illustrates the distribution of flux rope parameters for the entire population, as well as each of the individual populations discussed in Section 2. In general there is a broad distribution of values for each parameter, with a few distinct trends. Further, the trends for each individual population follow the overall trends with few exceptions.

From Fig. 4a, low amplitude ropes (10–20 nT) are most common, but flux ropes were identified having amplitudes as high as 100 nT. Flux ropes in population 3 (observed in darkness, where the ambient field is typically small) are more likely to have small amplitudes than other populations. The flux rope previously reported on the

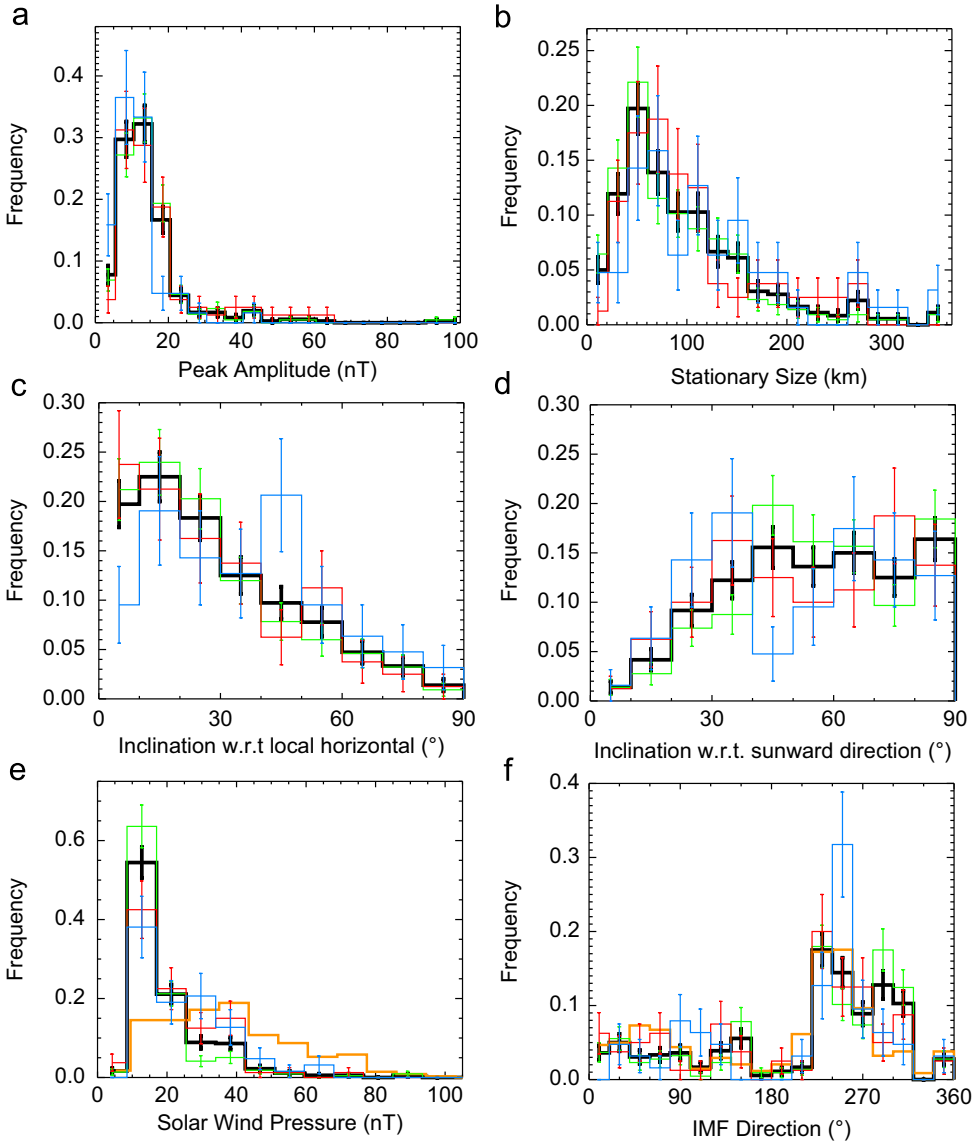

Fig. 4. Histograms showing the relative occurrence frequency of: (a) peak flux rope field amplitude, (b) flux rope stationary size, (c) flux rope inclination with respect to local horizontal, (d) flux rope inclination with respect to the sunward direction, (e) solar wind pressure proxy, and (f) interplanetary magnetic field draping direction. Colors (green, red, and blue) denote population (1, 2, and 3), and black denotes all flux rope populations. The orange histograms in (e) and (f) show the distribution for all MGS data (independent of the observation of flux ropes) during the four week interval. (For interpretation of the references to color in this figure legend, the reader is referred to the web version of this article.)

nightside also had weak peak field strength (Eastwood et al., 2008). The distribution of sizes (Fig. 4b) peaks at ~50 km and has a tail extending to higher values, with no significant differences between the populations. The distribution is similar to that obtained by Vignes et al. (2004). Note however that the previous study used only ropes in the northern hemisphere (similar to our population 1), and used the full width at half maximum to define the diameter (resulting in a lower peak value). Further, the observed flux ropes may be moving relatively quickly over the spacecraft and therefore may appear smaller than they are.

Flux ropes tend to be parallel to the Martian surface more often than perpendicular (Fig. 4c), and favor orientations orthogonal to the direction of solar wind flow (Fig. 4d). Individual populations do not differ significantly. We expect this trend for each of the populations, as this orientation seems likely to result from the formation mechanisms envisioned for each type of flux rope (cf. Luhmann and Cravens, 1991). Vignes et al. (2004) reported that the orientation of northern hemisphere (population 1, mostly) flux ropes was randomly distributed. To the contrary, we observe a significant depletion of ropes perpendicular to the local horizontal in all populations. The depletion is smaller for population 3, which is consistent with our association of this population with either reconnection in the tail current sheet, or with flux ropes transported far from their site of origin on the dayside. Our results are obtained for a single altitude and local time, unlike those of Vignes et al. (2004), but this difference is not likely to provide an explanation for the discrepancy.

We examine the two main external conditions that exist during flux rope formation and evolution: solar wind pressure and the draping direction of the Interplanetary Magnetic Field (IMF). The values obtained for these external conditions are both proxies obtained once per ~2 h MGS orbit (Brain et al., 2005, 2006), with high associated uncertainties. The background distributions of both proxies, i.e. the values associated with the entire four-week period examined, independent of the observation of flux ropes, are shown in orange in Fig. 4e and f. The distribution of IMF draping direction (Fig. 4f) during flux rope events does not vary significantly from the background distribution of IMF draping directions, indicating that

there is no particular draping direction that favors rope formation over others. This is true of all flux rope populations, and we have no reason to expect a dependence on IMF direction for populations 1 and 3. One might expect flux ropes in population 2 to be more likely to occur when the draped IMF is anti-parallel to crustal magnetic fields. This may be true, but the many crustal fields at Mars have a variety of orientations and polarities. Therefore flux ropes may form in some locations for one orientation of the IMF and other locations when the IMF rotates, so that the global production of flux ropes does not vary significantly.

However, from Fig. 4e it appears that ropes in all populations (especially population 1) are more likely to form when the solar wind pressure is relatively low. This result is consistent with those inferred by Vignes et al. (2004) for ionospheric flux ropes at Mars, and Russell and Elphic (1979) for Venus (see also Luhmann and Cravens, 1991). When the solar wind pressure is much greater than the ionospheric thermal pressure the solar wind magnetic field completely penetrates the atmosphere so that there is no magnetic shear between the ionosphere and overlying solar wind plasma, suppressing flux rope formation. But during periods of low solar wind pressure (and/or during periods of high ionospheric pressure, such as solar maximum) the solar wind magnetic field is excluded from the ionosphere, resulting in magnetic shear favorable for flux rope formation. However, flux ropes near crustal fields and current sheets at Mars are thought to result from magnetic reconnection (Eastwood et al., 2008). Halekas et al. (2009) demonstrated that current sheets with Hall magnetic field signatures (indicating reconnection) are more likely to be observed when solar wind pressure is higher than normal. Flux ropes near reconnection diffusion regions (reported mostly for the Martian nightside) are most likely to be represented by our population 3. This population, while distributed toward higher pressure than the other populations, is still biased toward low pressure time periods. This indicates either that magnetic islands like those of Eastwood et al. (2008) are not dominant in any of our three populations, that magnetic islands do not preferentially form during high pressure periods (even though reconnection is more likely), or that the reconnection process itself is not more likely to occur during high pressure periods.

We explore the correlations between various flux rope parameters in Fig. 5. Large flux ropes with fields greater than 30 nT are

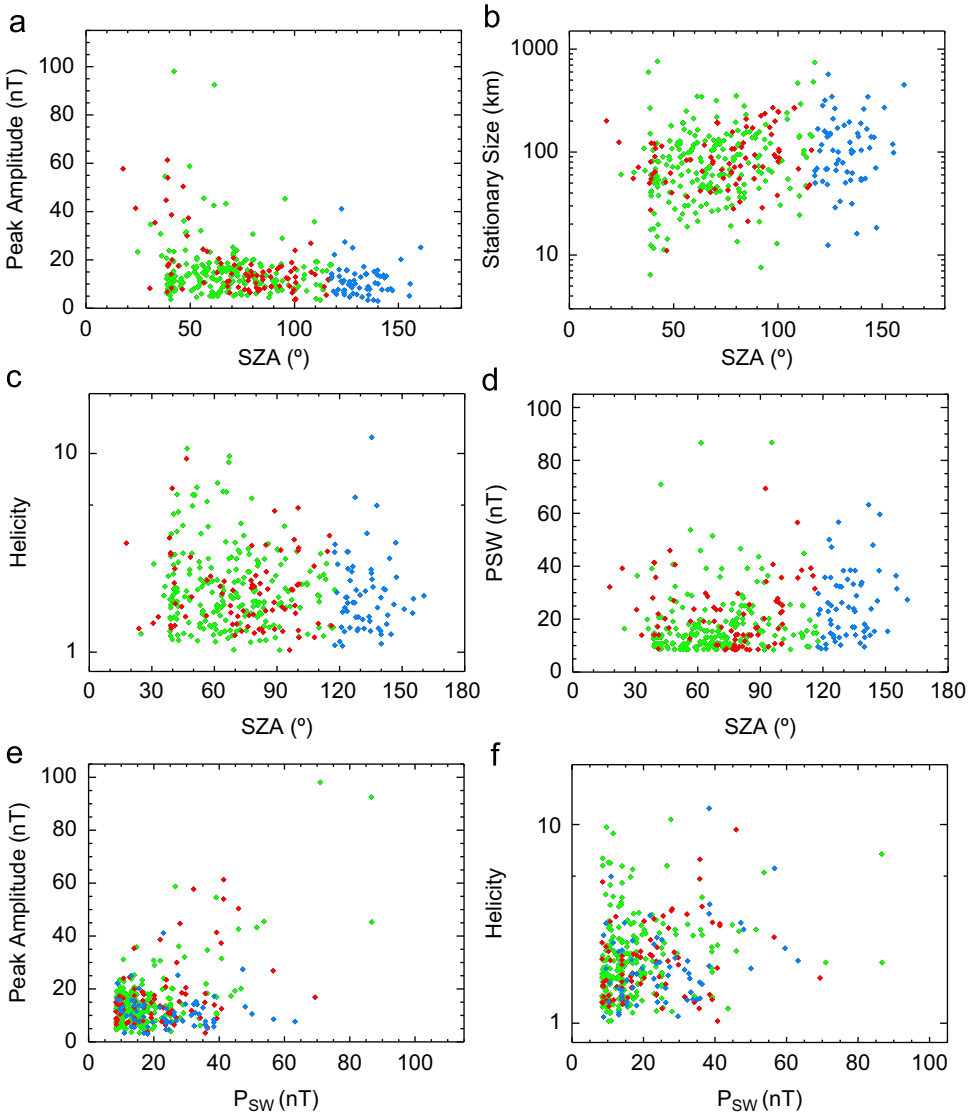

Fig. 5. Scatter plots comparing flux rope parameters: (a–d) peak amplitude, diameter, helicity, and solar wind pressure vs. solar zenith angle, and (e, f) peak amplitude and helicity vs. solar wind pressure. Colors denote the three flux rope populations as in Fig. 4. (For interpretation of the references to color in this figure legend, the reader is referred to the web version of this article.)

only observed for SZA less than 70° (Fig. 5a). This relationship between peak amplitude and solar zenith angle corroborates the findings of Vignes et al. (2004), and appears to hold for all three populations. Flux rope diameter increases with increasing solar zenith angle (Fig. 5b), and there is some suggestion that rope helicity decreases with solar zenith angle (Fig. 5c). Helicity trends with solar zenith angle and flux rope peak amplitude (not shown here) were noted by Vignes et al. (2004), though the trends evident in our flux rope database are weaker, and are less evident for flux ropes observed in darkness (population 3). As we discuss below, ionospheric and crustal-field-associated flux ropes may be mixed in populations 1 and 2 in our analysis. Taken together, the three trends in Fig. 5a–c imply either that flux ropes that form at different locations form with different properties (favoring larger peak amplitude, smaller diameter, and larger helicity near the subsolar point) and that we observe many flux ropes close to their point of origin, or that the characteristics of flux ropes evolve (becoming weaker, broader, and less 'stretched') as they are carried toward higher solar zenith angles.

The location at which flux ropes are observed appears to be independent of the solar wind pressure (Fig. 5d). The solar wind pressure is correlated with the peak amplitude of ropes observed in sunlight (red and green points in Fig. 5e), but does not strongly vary with the helicity of the ropes (Fig. 5f). While high solar wind pressure inhibits flux rope formation in general, those that do form tend to have larger amplitudes.

The similarity between the three populations, and especially between populations 1 and 2, is somewhat surprising. For example, we expected flux ropes observed near crustal fields to have larger amplitudes and diameters than the other populations. The similarity between populations 1 and 2 could indicate that the large strong flux ropes associated with crustal fields identified by Brain et al. (2010) and Morgan et al. (2011) are in actuality part of a continuum of crustal field-associated flux ropes having a variety of sizes and peak amplitudes. Alternatively, the similarity could indicate that flux ropes at Mars are observed well after their initial formation, and that flux ropes formed by different processes evolve toward the same distribution of physical states. Finally, the similarity could indicate that flux ropes formed by different processes (and having different physical characteristics) have been imperfectly separated into the three populations we defined based solely on the location of each event. For example, flux ropes formed at crustal fields may be observed far away, and be counted in our population 1 (and vice versa). Flux ropes that formed on the dayside may be observed in eclipse and be counted in our population 3. All of the above possibilities seem possible, and even likely.

The similarity in the stationary size and helicity distributions between populations 1 and 2, especially, suggest that separation of events into different populations is difficult. We would expect ionospheric flux ropes like those previously reported at Venus and Mars to be much smaller than 100 km, and to be tightly coiled (Luhmann and Cravens, 1991; Vignes et al., 2004). We note that relatively few flux ropes (presumably Venus-like) were reported at 400 km altitudes by Vignes et al. (2004). Our population 1 may contain a significant contribution from flux ropes formed near crustal fields that have propagated away, or ionospheric flux ropes at 400 km altitudes have characteristics that differ considerably from those previously reported for lower altitudes.

4. Summary and discussion

We used minimum variance analysis of MGS MAG data to identify 360 flux ropes over four one-week periods spanning a single year. All flux ropes were observed at 400 km altitudes and 2 am/2 pm local time. We observe that Martian flux ropes have mean 'stationary size' of ~80–100 km, mean peak field amplitude of ~15 nT, are commonly oriented at low angles relative to the local horizontal and at high angles relative to the solar wind flow. However, there is a broad distribution of flux rope parameters around these mean values. Flux ropes are observed preferentially during periods of low solar wind pressure, but show no dependence on IMF draping direction. Flux ropes observed at low solar zenith angles tend to have larger peak field amplitudes, smaller sizes, and larger helicities than ropes observed at larger solar zenith angles. Recalling that the measured peak field amplitude depends upon the distance the spacecraft passed from the center of the structure, one might expect the measured amplitudes to be slightly smaller at high solar zenith angles where the rope diameters are larger. Peak field amplitudes are also larger during periods of high solar wind pressure.

Since several types of flux rope have been reported at Mars, we separated flux ropes into three populations according to their location. The individual populations followed the trends noted above, with only a few exceptions. Flux ropes observed in darkness were more likely to have small peak field amplitudes, and dayside flux ropes observed far from crustal fields were more likely to be observed during periods of low solar wind pressure than the other populations (though all three populations had distributions that peaked during low pressure periods). Finally, flux ropes observed in darkness had uniformly low peak field amplitude, independent of the solar wind pressure.

The outflow of atmospheric ions is of particular interest at Mars and unmagnetized planets (e.g. Barabash et al., 2007a, 2007b), and flux ropes may provide a means of transporting ionospheric plasma away from the planet. Previously, Brain et al. (2010) roughly estimated the escape rate from very large crustal field-related flux ropes at Mars. Since the flux ropes reported in this work are observed in the ionosphere, they may be capable of removing atmosphere from Mars. However, we cannot be certain from the present set of observations which, if any, of the flux ropes actually do contribute to atmospheric escape or quantify the loss. Venus-like ionospheric flux ropes may form at the solar wind—ionosphere interface and transport sheath plasma inward, rather than ionospheric plasma outward. Flux ropes associated with stretched crustal fields appear to be filled with ionospheric plasma, but a number of relevant parameters are difficult to determine using the measurements from a single spacecraft, including the dimensions of the flux rope and whether it is detached. And flux ropes associated with reconnection in current sheets near Mars (especially on the nightside, downstream from the ionosphere) may not be involved with the removal of any ionospheric plasma.

For now, we feel that we must be content to estimate the occurrence rate of flux ropes. This rate appears to be quite variable on timescales of weeks, ranging from 32 to 219 identified flux ropes per week. Overall, we identified ~1 flux rope per ~2 h spacecraft orbit, and note that the spacecraft only sampled a small slice of the Martian plasma interaction region (and a small portion of this slice at any given time). Thus, it is reasonable to assume that flux ropes constantly form and are continuously present near Mars, depending upon external conditions. These observations emphasize that the Mars–solar wind interaction is highly dynamic and time-dependent. The ubiquity of flux ropes further suggests that modelers of Mars' interaction with the solar wind should strive to account for the features that we present above for flux ropes at ~400 km altitude at 2 am/2 pm local time: a spatial distribution of flux ropes that allows for their existence in both the Northern and Southern hemispheres, near and far from crustal fields, and in sunlight and eclipse; distributions in amplitude and stationary size that peak near 15 nT and ~100 km;

distributions in orientation weighted toward horizontal flux ropes perpendicular to the sunward direction; preferential flux rope formation at low solar wind pressures; variations in amplitude, size, and helicity with solar zenith angle; and a correlation between amplitude and solar wind pressure.

Pertinent lines of future investigation include consideration of a larger sample of MGS data (this study examined four weeks out of the 7 years of available observations), examination of extreme ultraviolet effects in the ionosphere, and consideration of solar storm effects. More work can also be done to separate the flux ropes more reliably into separate populations. Better separation might be achieved through consideration of the context of each event, rather than assignment to populations based solely on their location. However, such efforts are bound to be subjective. Detailed investigation of the charged particle populations present inside flux ropes could be undertaken in a future study. Plasma simulations (global or local) that include flux ropes would be quite useful for constraining flux rope formation mechanisms, locations, evolution, and lifetimes. Finally, new observations of flux ropes that combine vector magnetic field, electron, and ion observations in flux ropes and surrounding regions (such as those that should be available from the upcoming MAVEN mission) should prove invaluable to determining the processes by which flux ropes of different types form and evolve near Mars.

Acknowledgments

We acknowledge useful conversations with T. Cravens and C. Mazelle. This research was funded by NASA Grant #NNX08AK95G. JPE holds an STFC Advanced Fellowship at Imperial College London.

References

Acuña, M.H., Connerney, J.E.P., Wasilewski, P., Lin, R.P., Mitchell, D., Anderson, K.A., Carlson, C.W., McFadden, J., Reme, H.R., Mazelle, C., Vignes, D., Bauer, S.J., Cloutier, P., Ness, N.F., 2001. Magnetic field of Mars: summary of results from the aerobraking and mapping orbits. J. Geophys. Res. 106 (E10), 23,403–23417.

Barabash, S., Fedorov, A., Lundin, R., Sauvaud, J.A., 2007a. Martian atmospheric erosion rates. Science 315 (5811), 501–503. doi:10.1126/science.1134358.

Barabash, S., Sauvaud, J.A., Gunell, H., Andersson, H., Grigoriev, A., Brinkfeldt, K., Holmström, M., Lundin, R., Yamauchi, M., Asamura, K., Baumjohann, W., Zhang, T.L., Coates, A.J., Linder, D.R., Kataria, D.O., Curtis, C.C., Hsieh, K.C., Sandel, B.R., Fedorov, A., Mazelle, C., Thocaven, J.J., Grande, M., Koskinen, H.E.J., Kallio, E., Säles, T., Riihela, P., Kozyra, J., Krupp, N., Woch, J., Luhmann, J., McKenna-Lawlor, S., Orsini, S., Cerulli-Irelli, R., Mura, M., Milillo, M., Maggi, M., Roelof, E., Brandt, P., Russell, C.T., Szego, K., Winningham, J.D., Frahm, R.A., Scherrer, J., Sharber, J.R., Wurz, P., Bochsler, P., 2007b. The analyser of space plasmas and energetic atoms (ASPERA-4) for the Venus express mission. Planet. Space Sci. 55 (12), 1772–1792.

Brain, D.A., Bagenal, F., Acuña, M.H., Connerney, J.E.P., 2003. Martian magnetic morphology: contributions from the solar wind and crust. J. Geophys. Res. 108 (A12), 1424. doi:10.1029/2002JA009482.

Brain, D.A., Halekas, J.S., Lillis, R., Mitchell, D.L., Lin, R.P., Crider, D.H., 2005. Variability of the altitude of the Martian sheath. Geophys. Res. Lett. 32, L18203. doi:10.1029/2005GL023126.

Brain, D.A., Mitchell, D.L., Halekas, J.S., 2006. The magnetic field draping direction at Mars from April 1999 through August 2004. Icarus 182, 464–473. doi:10.1016/j.icarus.2005.09.023.

Brain, D.A., Baker, A.H., Briggs, J.A., Eastwood, J.P., Halekas, J.S., Phan, T.-D., 2010. Episodic detachment of Martian crustal magnetic fields leading to bulk escape. Geophys. Res. Lett. 37, L14108. doi:10.1029/2010GL043916.

Bulraga, L., Sittler, E., Mariana, F., Schwenn, R., 1981. Magnetic loop behind an interplanetary shock—Voyager, Helios, and IMP 8 observations. J. Geophys, Res. 86 (A8), 6673–6684.

Cain, J.C., Ferguson, B.B., Mozzoni, D., 2003. An $n=90$ internal potential function of the Martian crustal magnetic field. J. Geophys. Res. 108 (E2), 5008. doi:10.1029/2000JE001487.

Cloutier, P.A., Law, C.C., Crider, D.H., Walker, P.W., Chen, Y., Acuña, M.H., Connerney, J.E.P., Lin, R.P., Anderson, K.A., Mitchell, D.L., Carlson, C.W., McFadden, J., Brain, D.A., Reme, H., Mazelle, C., Sauvaud, J.A., d'Uston, C., Vignes, D., Bauer, S.J., Ness, N.F., 1999. Venus-like interaction of the solar wind with Mars. Geophys. Res. Lett. 26 (17), 2685–2688.

Eastwood, J.P., Balogh, A., Dunlop, M.W., Horbury, T.S., Dandouras, I., 2002. Cluster observations of fast magnetosonic waves in the terrestrial foreshock. Geophys. Res. Lett. 29 (22), 2046. doi:10.1029/2002GL015582.

Eastwood, J.P., Sibeck, D.G., Slavin, J.A., Goldstein, M.L., Lavraud, B., Sitnov, M., Imber, S., Balogh, A., Lucek, E.A., Dandouras, I., 2005. Observations of multiple X-line structure in the Earth's magnetotail current sheet: a cluster case study. Geophys. Res. Lett. 32, L11105. doi:10.1029/2005GL022509.

Eastwood, J.P., Phan, T.-D., Mozer, F.S., Shay, M.A., Fujimoto, M., Retino, A., Hesse, M., Balogh, A., Lucek, E.A., Dandouras, I., 2007. Multi-point observations of the Hall electromagnetic field and secondary island formation during magnetic reconnection. J. Geophys. Res. 112, A06235. doi:10.1029/2006JA012158.

Eastwood, J.P., Brain, D.A., Halekas, J.S., Drake, J.F., Phan, T.D., Øieroset, M., Mitchell, D.L., Lin., R.P., Acuña, M., 2008. Evidence for collisionless magnetic reconnection at Mars. Geophys. Res. Lett., 35. doi:10.1029/2007GL032289.

Elphic, R.C., Cattell, C.A., Takahashi, K., Bame, S.J., Russell, C.T., 1986. ISEE 1 and 2 observations of magnetic flux ropes in the magnetotail: FTE's in the plasma sheet? Geophys. Res. Lett. 13 (7), 648–651.

Halekas, J.S., Eastwood, J.P., Brain, D.A., Phan, T.D., Øieroset, M., Lin, R.P., 2009. In situ observations of reconnection Hall magnetic fields at Mars: evidence for ion diffusion region encounters. J. Geophys. Res. 114, A11204. doi:10.1029/2009JA014544.

Harnett, E.M., 2009. High-resolution multifluid simulations of flux ropes in the Martian magnetoshpere. J. Geophys. Res. 114, AO1208. doi:10.1029/2008JA013648.

Hones, E.W., Birn, J., Baker, D.N., Bame, S.J., Feldman, W.C., McComas, D.J., Zwickl, R.D., Slavin, J.A., Smith, E.J., Tsurutani, B.T., 1984. Structure of the magnetotail at $220R_E$ and its response to geomagnetic activity. Geophys. Res. Lett. 11 (10), 1046–1049.

Jackman, C.M., Russell, C.T., Southwood, D.J., Arridge, C.S., Achilleos, N., Dougherty, M., 2007. Strong rapid dipolarizations in Saturn's magnetotail: in situ evidence of reconnection. Geophys. Res. Lett. 34, L11203. doi:10.1029/2007GL029764.

Jackman, C.M., Arridge, C.S., Krupp, N., Bunce, E.J., Mitchell, D.G., McAndrews, H.J., Dougherty, M., Russell, C.T., Achilleos, N., Jones, G.H., Coates, A.J., 2008. A multi-instrument view of tail reconnection at Saturn. J. Geophys. Res. 113, A11213. doi:10.1029/2008JA013592.

Knetter, T., Neubauer, F.M., Horbury, T., Balogh, A., 2004. Four-point discontinuity observations using cluster magnetic field data: a statistical survey. J. Geophys. Res. 109, A06102. doi:10.1029/2003JA010099.

Kronberg, E.A., Woch, J., Krupp, N., Lagg, A., Khurana, K.K., Glassmeier, K.-H., 2005. Mass release at Jupiter: substorm-like processes in the Jovian magnetotail. J. Geophys. Res. 110, A03211. doi:10.1029/2004JA010777.

Ledvina, S.A., Nunes, D.C., Cravens, T.E., Tinker, J.L., 2002. Pressure balance across magnetic flux ropes in the ionosphere of Venus. J. Geophys. Res. 107 (A6), 1074. doi:10.1029/2001JA900147.

Lepping, R.P., Jones, J.A., Burlaga, L.F., 1990. Magnetic field structure of interplanetary magnetic clouds at 1 AU. J. Geophy. Res. 95 (A8), 11957–11965.

Luhmann, J.G., 1990. 'Wave' Analysis of Venus Ionospheric Flux Ropes. Physics of Magnetic Flux Ropes. AGU Monograph, AGU, Washington, DC.

Luhmann, J.G., Cravens, T.E., 1991. Magnetic fields in the ionosphere of Venus. Space Sci. Rev. 55, 201–274.

Mitchell, D.L., Lin, R.P., Rème, H., Crider, D.H., Cloutier, P.A., Connerney, J.E.P., Acuña, M.H., Ness, N.F., 2000. Oxygen Auger electrons observed in Mars' ionosphere. Geophys. Res. Lett. 27 (13), 1871–1874.

Moldwin, M.B., Phillips, J.L., Gosling, J.T., Scime, E.E., McComas, D.J., Barne, S.J., Balogh, A., Forsyth, R.J., 1995. Ulysses observations of a noncoronal mass ejection flux rope: evidence of interplanetary magnetic reconnection. J. Geophys. Res 100 (19), 903–910.

Morgan, D.D., DGurnett, D.A., Akalin, F., Brain, D., Leisner, J.S., Duru, F., Frahm, R.A., Winningham, J.D., 2011. Dual-spacecraft observation of large-scale magnetic flux ropes in the Martian ionosphere. J. Geophys. Res., 116, A02319. doi:10.1029/2010JA016134.

Russell, C.T., Elphic, R.C., 1978. Initial ISEE magnetometer results—magnetopause observations. Space Sci. Rev. 22, 681–715.

Russell, C.T., Elphic, R.C., 1979. Observations of magnetic flux ropes in the Venus ionosphere. Nature 279 (5714), 616–618.

Sibeck, D.G., Siscoe, G.L., Slavin, J.A., Smith, E.J., Bame, S.J., Scarf, F.L., 1984. Magnetotail flux ropes. Geophys. Res. Lett. 11 (10), 1090–1093.

Slavin, J.A., Lepping, R.P., Gjerloev, J., Fairfield, D.H., Hesse, M., Owen, C.J., Moldwin, M.B., Nagai, T., Ieda, A., Mukai, T., 2003. Geotail observations of magnetic flux ropes in the plasma sheet. J. Geophys. Res. 108 (A1), 1015. doi:10.1029/2002JA009557.

Slavin, J.A., Acuna, M.H., Anderson, B.J., Baker, D.N., Benna, M., Boardsen, S.A., Gloeckler, G., Gold, R.E., Ho, G.C., Korth, H., Krimigis, S.M., McNutt Jr., R.L., Raines, J.M., Sarantos, M., Schriver, D., Solomon, S.C., Travnicek, P., Zurbuchen, T.H., 2009. MESSENGER observations of magnetic reconnection in Mercury's magnetosphere. Science 324. doi:10.1126/science.1172011.

Sonnerup, B.U.Ö., Cahill Jr., L.J., 1967. Magnetopause structure and attitude from Explorer 12 observations. J. Geophys. Res. 72, 171–183.

Vignes, D., Acuña, M.H., Connerney, J.E.P., Crider, D.H., Reme, H., Mazelle, C., 2004. Magnetic flux ropes in the Martian atmosphere: global characteristics. Space Sci. Rev. 111 (1-2), 223–231. doi:10.1023/B:SPAC.0000032716.21619.f2.

Walker, R.J., Russell, C.T., 1985. Flux transfer events at the Jovian magnetopause. J. Geophys. Res. 90 (A8), 7397–7404.

Wei, H.Y., Russell, C.T., Zhang, T.L., Dougherty, M.K., 2010. Comparison study of magnetic flux ropes in the ionospheres of Venus, Mars and Titan. Icarus 206 (1), 174–181. doi:10.1016/j.icarus.2009.03.014.